# Structural and Dynamical Properties of Polystyrene Thin Films Supported by Multiple Graphene Layers

**ARTICLE** *in* MACROMOLECULES · APRIL 2015

Impact Factor: 5.8 · DOI: 10.1021/ma502524e



**2 AUTHORS:**

Anastassia N. Rissanou
University of Crete
**30** PUBLICATIONS **164** CITATIONS

SEE PROFILE

V. A. Harmandaris
University of Crete
**59** PUBLICATIONS **1,900** CITATIONS

SEE PROFILE

Macromolecules

Article

pubs.acs.org/Macromolecules

# Structural and Dynamical Properties of Polystyrene Thin Films Supported by Multiple Graphene Layers

Anastassia N. Rissanou*,†,‡ and Vagelis Harmandaris*,†,‡

†Institute of Applied and Computational Mathematics (IACM), Foundation for Research and Technology Hellas (FORTH), GR-71110 Heraklion, Crete Greece

‡Department of Mathematics and Applied Mathematics, University of Crete, GR-71409, Heraklion, Crete Greece

Supporting Information

**ABSTRACT:** We explore the effect of the number of graphene layers on the structural and dynamical properties of a free-standing polystyrene film supported by multiple graphene sheets. Detailed atomistic molecular dynamics simulations have been performed for systems with one up to four graphene sheets. Our purpose is to highlight the way that the two (PS/graphene and PS/vacuum) interfaces affect the various properties of the PS thin film as a result of the different (PS/graphene) adhesive interaction strength. Both graphene and vacuum affect the various properties of the polymer, though in a different way. Mass density profiles present an increasing maximum density peak, as the number of the graphene layers increases. Structural analysis highlights a tendency for an almost parallel to the graphene surface orientation of the phenyl rings at distances ($r$) very close to graphene whereas at the vacuum interface phenyl rings stick out into the vacuum phase in an almost perpendicular orientation. This behavior is similar for all four systems. On top of that clear dynamical heterogeneities due to polymer/graphene and polymer/vacuum interfaces have been observed in the level of both segmental and terminal dynamics. Four regimes for the segmental orientational dynamics of the PS chains are observed: (a) Polymer chains very close (up to ∼0.3−0.4 nm) to the graphene layers exhibit an average segmental relaxation time about 4 orders of magnitude larger than that of the bulk system. In this region the more the graphene layers, the slower the dynamics. (b) Chains at longer distances (up to ∼3−4 nm) show a considerable slowdown of chain dynamics with respect to the bulk PS systems. (c) A "bulk-like" regime follows (distances ∼4.0−9.5 nm) where the chain segmental dynamics only slightly depends on $r$. Finally, (d) a regime (∼9.5−13 nm) with much faster PS chain mobility at the PS/vacuum interface appears.

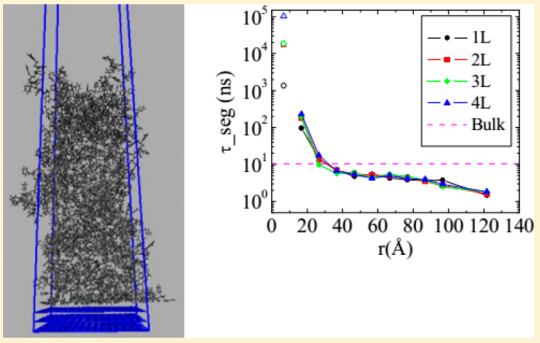


## 1. INTRODUCTION

Polymer/graphene nanostructured systems have attracted great scientific attention the past years for both scientific and technological reasons. Indeed, due to the exceptional physical properties of graphene (such as its electronic transport properties,[1] mechanical properties,[2] high thermal and electrical conductivity, impermeability for all gas molecules and transparency, etc.),[3,4] hybrid polymer/graphene materials are very promising candidates for a broad range of possible applications.[3,5]

Because of the above reasons, the study of graphene-based polymer nanostructured systems is an intense research area. From the scientific point of view the main challenge is to study such nanostructured systems at the molecular level and predict their structure−properties relations. A particular important question concerns the way the polymer/graphene interface affects the properties of the polymer chains, as well as the estimation of the width of the interphase, based on the specific property under study.[6] The latter is directly related with the more general research field of polymer/solid interfaces, which has been studied extensively in the past through theoretical approaches,[7,8] experiments,[9−13] and simulation works.[14−20] Although this is a well-studied research area there are still open questions, especially related to the dynamical behavior and the relaxation processes of polymers at surfaces and interfaces. For example, the effect of the polymer/solid interface on the glass transition temperature of a polymer thin film is a much argued topic.[21−25]

Even more, free-standing (supported) polymer films, where the two, polymer/substrate and polymer/air or polymer/vacuum, interfaces compete with each other, are of particular interest. Because of this reason, there are many studies that focus on the thickness of the interphases for various properties of a polymer film.[17,22,26−30] A much debated issue is the dynamical behavior of the polymeric chains as a function of the thickness of the film. Experiments reported an anomalous dynamics at the interfaces which persists for a few nanometers[21,31,32] or even tens of nanometers;[9,10] in addition, long-range effects were observed in the films which affect the glass transition temperature.[9,10,23,33] The two- and three-layer

Received: December 16, 2014
Revised: March 13, 2015





DOI: 10.1021/ma502524e
Macromolecules XXXX, XXX, XXX−XXX

models have been used in order to interpret this behavior, assuming different viscosity for the various layers and strong hydrodynamic interactions between the interfacial layer and the remaining film.[31,34]

More specifically for polymer films supported by graphene or graphite there are various molecular simulation studies that explore the effect of the interfaces on both structural and dynamical properties of the polymer molecules.[14−18,29,35−39] For example, Tatek et al.[38] studied the structural properties of atactic polystyrene supported by three different substrates: a-quartz, graphite, and amorphous silica. Based on atomistic molecular dynamics simulations, their results revealed the differences in the structural properties and the density for the three types of surfaces. Several simulation works of polymer/graphite, or polymer/graphene, systems have shown that the dynamics of the adsorbed molecules perpendicular to the surface is quantitatively and qualitatively different from that in the bulk. Especially for the segmental diffusion a strong dependence on the thickness of the layer next to graphite has been reported; i.e., the closer the polymer chains to the graphene, the slower its segmental mobility.[15−19,29]

All the above studies render the role of the substrate crucial for the various properties of hybrid polymer nanostructured materials. Many factors such as the adsorption polymer/substrate interaction strength, the roughness of the surface, the film thickness, and the viscosity of the polymer chains designate the interphase for each specific property. A very interesting study of Hanakata et al.[26] based on coarse-grained molecular dynamics simulations reveals the role of the film thickness and substrate interactions on film dynamics for supported polymer films on rough or smooth surfaces. It was found that the relaxation time of the film on the smooth surface decreases as the film thickness is decreased, relative to the corresponding bulk values, and this behavior is more pronounced for lower temperatures. An opposite behavior was found for rough surfaces. Moreover, the glass transition temperature of polymer film increases with decreasing film thickness on a rough surface relative to the bulk value, while for a smooth surface the trend is opposite. Finally, a relation between the interfacial area and a collective molecular motion in the film is found. The same topic is also studied by Lang et al.,[40] through molecular dynamics simulations on a freestanding polymer film. It was found that cooperatively rearranging regions facilitate propagation of interfacial dynamics further into the film at temperatures around the glass transition temperature.

Furthermore, the substantial role in the formation of graphene-based polymer nanocomposites plays the exfoliation of graphite's layered structure and its dispersion in a polymer matrix.[4] For example, in many experimental studies multiple graphene, or functionalized graphene (i.e., graphene oxide), layers have been used, rather than a single atomic layer of exfoliated graphene, in order to improve adhesion between graphene and polymer chains.[41]

With reference to the above discussion it is of high interest to study the properties of polymer thin films supported by multiple graphene layers at the molecular level. For such systems polymer/vacuum (or polymer/air) interface is also expected to play an important role in the final properties of the hybrid systems. Very recently, we have studied the structural and dynamical properties of various polymers (polyethylene, PE, polystyrene, PS, and poly(methyl methacrylate), PMMA) confined between two graphene layers.[14,16] For all systems segmental dynamics of the polymer chains, quantified through the segmental relaxation time, $\tau_{seg}$, is much slower close to the graphene layer, compared to the bulk one. In addition, $\tau_{seg}$ decreases as the distance from the graphene layer increases, reaching a plateau value in the bulk region, identical to the value which stands for the corresponding bulk systems.

In the current study we extend the previous works by exploring the effect of the number of graphene layers on the structural and dynamical properties of a free-standing polystyrene film supported by multiple (from one up to four) graphene sheets. Our purpose is to highlight the way that the two (PS/graphene and PS/vacuum) interfaces affect the various properties of the PS thin film, for the systems with various numbers of graphene sheets, as a result of the different (PS/graphene) adhesive interaction strength because of the additional graphene sheets. The rest of the paper is organized as follows: The model and the simulation method are described in section 2. Section 3 contains the results and the corresponding discussion, separating in subsections concerning the properties under investigation. Finally, our conclusions are presented in section 4.

## 2. MODEL AND SIMULATION METHOD

In the present work we study a thin atactic polystyrene, PS, film (96 10-mer chains) supported by graphene layers. Four different systems were set up where the polymer film is supported by one (1L), two (2L), three (3L), and four (4L) graphene layers. The free surface is exposed to vacuum. We performed atomistic molecular dynamics (MD) simulations using an all-atom model for polystyrene. Simulations were carried out in the NVT canonical ensemble at 1 atm and 500 K with the GROMACS package.[42] The temperature was kept constant using the stochastic velocity rescaling thermostat.[43] Details about the atomistic force field of PS can be found in previous works.[18,44] For the interaction between polymer atoms and graphene layers the Lorentz−Berthelot rules have been used. The nonbonded interaction of the graphene carbons were taken from a potential used for graphite: $\varepsilon_{cc}/k_B$ = 28 K and $\sigma_{cc}$ = 3.4 Å.[45] The lattice constant of the graphene layers is equal to 2.462 Å. A cutoff distance of 1.5 nm has been used for both electrostatic and Lennard-Jones (LJ) interactions. Note here that the choice of a quite large cutoff for the van der Waals and Coulomb interactions is necessary in order to take into account the interfacial structure (i.e., inhomogeneous polymer density). In order to use a typical cutoff used in atomistic simulations ( ∼ 1 nm), a special treatment for the tail corrections has to be incorporated due to the density inhomogeneities of polymer thin films. Here we use a quite large cutoff beyond which these corrections are negligible.[17,18,35] Periodic boundary conditions, which have been applied in all three directions of the simulation box, ensure infinite graphene layers with no edges. In the current study graphene has been represented as a set of LJ carbon atoms, centered at their crystallographic positions which remain fixed in space during the simulation and are eclectrically neutral. The first sheet is placed at the bottom of the simulation box and the rest of them at distances multiples of 0.335 nm (i.e., thickness of one graphene layer). The thickness of the polymer film is about 12 nm, and its lateral dimension is (4.26 × 3.69) nm$^2$, whereas the bulk radius of gyration ($R_g$) is about 0.7 Å. An important issue in all molecular simulations concerns possible finite size effects due to rather small, compared to experimentally relevant, model systems. Here, such effects might be associated with the lateral in plane dimensions of the simulation box, especially if we consider long-range phenomena


DOI: 10.1021/ma502524e
Macromolecules XXXX, XXX, XXX−XXX

such as cooperative length scales of dynamics[26,46,47] and/or percolation effects.[48,49] In order to ensure that finite size effects do not exist in our systems, we have simulated a system with the double lateral dimension (i.e., (8.52 × 7.38) nm$^2$) for the case with one graphene layer. Results concerning the density profile as well as the autocorrelation function $P_2(t)$ of the $\mathbf{v}_{bb}$ vector are shown in Figures 2s and 3s of the Supporting Information. No differences between the two systems, within the statistical accuracy, are observed.

Simulation runs for all systems were performed for 200 ns after the equilibration, and statistics of 2000 configurations were gathered. Equilibration of polymer chains is in general a nontrivial issue. In our study, in order to equilibrate the systems, we first performed MD simulations at high temperature (i.e., 700 K) until decorrelation of the end-to-end vector is succeeded. Then, annealing up to 500 K with various cooling rates was performed in order to check the effect of the cooling rate on the properties of the final system. No strong effect on the cooling rate was found. Here we report data using a cooling rate of 10 K/ns. Afterwards, NPT simulations of 100 ns were performed in order to attain a "constant" density value. Finally, statistics was gathered from the production runs, which were performed in the NVT statistical ensemble for another 200 ns. Equilibration at high temperature was determined from the autocorrelation function ($u(t)$) of the end-to-end vector ($\mathbf{R}_{ee}$) at $T$ = 700 K, which is presented in Figure 4s of the Supporting Information. A complete decorrelation of $\mathbf{R}_{ee}$ is observed even at the closest to the graphene distances (first and second adsorption layers).

Note also that test runs for a supported polymer film with one flexible graphene layer (i.e., using a full force field, including intramolecular terms, for graphene[50]) has been performed. Preliminary analysis has shown that there are differences between frozen and flexible graphene layers, especially at the first adsorption layer. A detailed investigation of the surface "softness" requires a number of additional extensive simulations. This will be a part of a future work.

Data analysis of the atomistic configurations, gathered during the MD simulations, has been performed using three different ways of division of the space across the model films (binning) depending on the analyzed quantity. First, for monomer mass density profiles a very detailed binning was performed. Space was divided into equal width bins of size 0.5 Å. Second, for structural information (i.e., second rank bond order parameter, $P_2(\cos\theta)$) a differentiation between vectors in the segmental and the molecular level exists. The former were analyzed using a 5 Å binning while the latter with a 10 Å binning because of their longer extension (i.e., end-to-end vector). Third, wider adsorption layers with respect to graphene, of about 10 Å, were used for the analysis of dynamics (autocorrelation functions and mean squared displacements) in both segmental and terminal levels. Overall, the choice of the proper "binning" size is a compromise between detailed information at the molecular level and accurate estimation of the specific property under study. Moreover for the analysis of the dynamical properties in both the segmental and molecular level, we have used a convention (C1) where the monomer/chain is classified to a specific distance (i.e., adsorption layer) from the surface according to the initial position of its center of mass (i.e., $t$ = 0 ps). An alternative convention (C2) could be the observation of the specific monomer/chain only for the time period that it belongs to the corresponding analysis regime. A comparison between the two analysis schemes has been made for the autocorrelation function of the $\mathbf{v}_{bb}$ vector of the 1L system. Small quantitative differences are found, as depicted in Figure 5s of the Supporting Information.

We should note here that glass transition temperature of bulk (high molecular weight) PS is about 360 K. Furthermore, a detailed comparison of the specific all-atom PS model at bulk has shown that the model predicts very well the qualitative dependence of relaxation times on temperature; however the dynamics of PS chains is slower (a factor of about 4.5 for all temperatures), compared to experimental data from dielectric spectroscopy.[51] This leads to a slight overestimation of the bulk PS glass transition temperature, $T_g$, estimated through an extrapolation of relaxation time in 100 s, with the current model, compared to the experimental one. A more detailed analysis of the dynamics of PS/graphene interfacial systems at different temperatures related to nanoconfinement effects on relaxation dynamics and the glass transition as well an estimation of the relevant characteristic temperatures (i.e., $T_g$, the onset temperature of the glass transition, $T_A$, and the mode-coupling temperature, $T_c$) of the current model will be the subject of a future work.

## 3. RESULTS AND DISCUSSION

As discussed above, a main goal of the present work is to study the effect of the different number of graphene layers on the properties of free-standing polystyrene/graphene thin films. The origin of such differences is expected to be directly related to the PS/graphene (attractive) interaction energy. This is further related to the work of adhesion at the polymer/graphene interface. There are several works in the literature that have explicitly characterized a dependence of $T_g$ on this property in supported and sandwiched films.[40,46,52,53] The increase of the strength of the interaction between the graphene layer(s) and the polymer matrix, as the number of the graphene layers increases, is presented in Figure 1. In this graph the

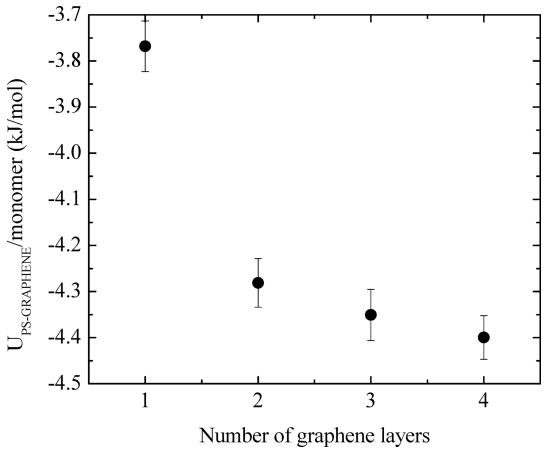


**Figure 1.** Average potential energy per monomer as a function of the number of graphene layers.

average (potential) energy per monomer, $U_{PS\text{-}Graphene}$, that describes the nonbonded dispersion interaction between the surface and the PS matrix is shown. In practice, graphene layers directly interact only with the amount of polymer, which lies in a distance smaller than 1.5 nm (i.e., cutoff distance of the LJ interactions) from the closest graphene layer. As expected, the more the graphene layers, the lower the $U_{PS\text{-}Graphene}$ value (i.e., the stronger the PS/graphene attraction). In addition, as the


DOI: 10.1021/ma502524e
Macromolecules XXXX, XXX, XXX−XXX

number of the graphene layers increases, the attraction converges toward a constant value, which indicates that a further increase of the number of graphene layers (i.e., beyond 4) would practically not expect to affect the properties of the polymer film.

**a. Density.** We first present data concerning the mass density profile of the polystyrene chains as a function of the distance from the graphene layers. To analyze polymer configurations, we divide space across the model films into bins separated by planes parallel to the graphene layers, of width equal to 0.5 Å. Within each bin, density values for each system were obtained by averaging over all configurations accumulated in the course of the atomistic MD simulation.

Average mass density of polystyrene chains $\rho(r)$, based on the monomer center of mass, is presented in Figure 2 for the

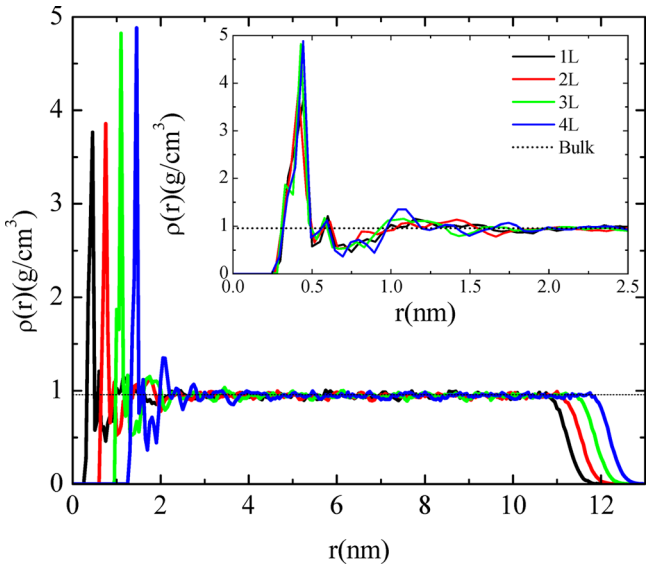


**Figure 2.** Mass monomer density profiles of PS for all four systems as a function of the distance ($r$) from the closest to the polymer film graphene layer. Inset: mass monomer density profiles of PS rescaled in $r$ by setting zero the closest graphene layer.

four model systems studied here. The density of all systems exhibits a qualitatively similar behavior; there is a region of high polymer density close to the graphene layers, a bulk-like regime follows, and then a gradual decrease of the polymer density at the polymer/vacuum interface appears. A detailed comparison between the four systems exhibits slight differences only in the first high-density regime. In this regime, which is extending in distances of only about 0.3−0.4 nm from the closest graphene layer, the density of PS chains is about 4−5 times larger than their bulk value. In addition, systems with more graphene layers exhibit larger maximum density peaks. This is not surprising if we consider the bigger attraction that is exerted on the polymer film as the number of the graphene layers increases due to the graphene/PS dispersion (van der Waals) interactions (see also Figure 1). We should also note that error bars in the density profile very close to the graphene layers are rather large due to the very slow chain mobility at the graphene/PS interface, as it will be discussed below. For longer distances, in the intermediate region between the two interfaces (about 2−10 nm) all systems attain the corresponding bulk density, which is represented with the horizontal dashed line. Finally, at the PS/vacuum interface the density of PS monomers drops gradually to zero, following a sigmoidal shape typical of a free surface polymer film.[17,54−56]

Overall, the effect of the number of graphene layers on the mass density distribution is strong only for the region very close to the graphene layers, i.e., in the first few (3−4) Å. This is particularly evident in the inset of Figure 2, where a rescaling of all curves in $r$ has been performed, by setting zero the closest graphene layer, in order to compare directly the density profiles of the four systems at the graphene/PS interface. In the following analysis we further use such a rescaling in order to directly (quantitatively) compare the four model systems studied here.

We further analyze the density profile of the polystyrene chains by calculating mass density distributions of the end and the inner parts of the polymer chain. Here, the "end part" concerns two monomers, the first and the last one, while the "inner part" is defined as the monomers of the chain in the interval $[(N/2-2)-(N/2+2)]$, where $N$ is the total number of monomers per chain. The density profiles of the end and the inner monomers, as a function of the distance from the closest graphene layer, are depicted in Figures 3a and 3b, respectively.

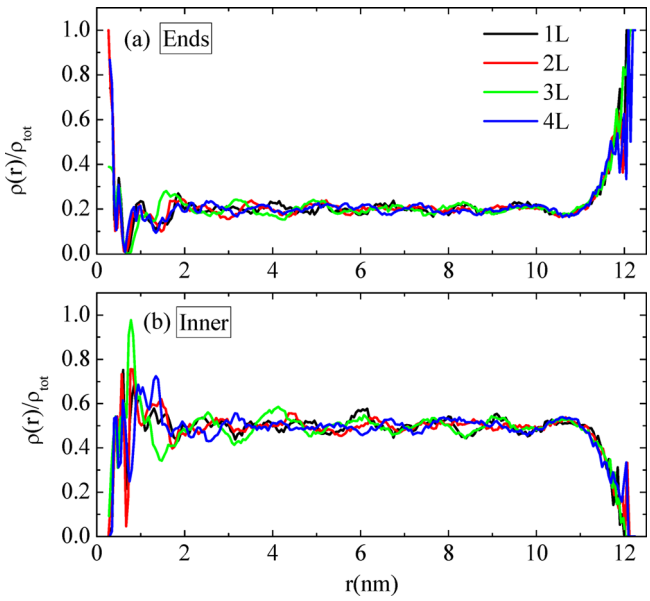


**Figure 3.** Mass monomer density profiles of PS for all four systems as a function of the distance ($r$) from the closest to the polymer film graphene layer for (a) end monomers and (b) inner monomers.

Data have been further normalized with the corresponding total density profile. On the one hand, the preference of the end monomers to lie on both interfaces is apparent for all systems. In addition, this preference is the same for the graphene layer and the vacuum as can be read from the density values at the corresponding distances. Also, there are not any substantial differences in the density profiles of end monomers among the four systems. On the other hand, the behavior of the inner monomers is complementary to that of the ends as can be seen in Figure 3b. Inner monomers prefer to stay in the middle of the film with similar density profiles for all systems. Such a behavior of the polymer chains has been also observed before,[17] for other polymer/solid interfacial systems, and it has an entropic origin: there is a larger entropic penalty for the inner part of the polymer chain to come close to a solid surface compared to the chain ends.



DOI: 10.1021/ma502524e
Macromolecules XXXX, XXX, XXX−XXX

**b. Structure of Polystyrene Chains.** We continue the analysis of the free-standing PS/graphene films by examining segmental as well as overall chain orientation tendencies. In more detail, we calculate the second rank bond order parameter,[57,58] $P_2(\cos\theta) = (3/2)\langle\cos^2\theta\rangle - 1/2$, where $\theta$ is the angle between an arbitrary vector, which is defined along the molecule, and one Cartesian axis. This order parameter provides detailed information for the orientation of individual parts of the polymer chain: limiting $P_2(\cos\theta)$ values of −0.5, 0.0, and 1.0 correspond to perfectly parallel, random, and perpendicular vector orientations relative to the planar surface, respectively.

Here we have calculated $P_2(\cos\theta)$ for two vectors, the end-to-end vector ($\boldsymbol{R}_{ee}$), which describes the backbone of the entire polymer chain, and the vector from the carbon attached to the backbone and a carbon which belongs to the phenyl ring ($\boldsymbol{v}^{phb}$). A schematic representation of $\boldsymbol{v}^{phb}$ vector is depicted on the sketch of polystyrene dimer in Figure 5a. For both vectors the $z$-axis was chosen, which is normal to the surface, in order to characterize chain orientation as a function of distance from the graphene layers.

Results for $P_2(\cos\theta)$ of $\mathbf{v}^{phb}$ and $\mathbf{R}_{ee}$ vectors as a function of the distance from the closest to the polymer graphene layer are presented in Figures 4a and 4b, respectively. First, $P_2(\cos\theta)$ data for the $\mathbf{v}^{phb}$ vector are shown in Figure 4a. The side (phenyl) groups of polystyrene lie almost parallel to the graphene layers for distances of about ∼5 Å (i.e., of the order of the thickness of one graphene layer, which is 3.35 Å), whereas for longer distances orientation of the phenyl groups becomes random. However, at the extreme region of the melt (i.e., vacuum interface), there is a clear tendency for the PS side groups to stick out into the vacuum phase in an almost perpendicular orientation. This behavior has also been reported in previous simulation studies[38,59] as well as in experimental observations.[60,61] This tendency of the bulky PS should be apparently related to a minimization of the free energy of the PS chains at the PS/vacuum interface. However, as also pointed out in ref 61, it is unclear whether it is of more energetic (due to chains cohesive interaction) or entropic origin. Even more, it is directly coupled with the end-to-end (backbone) vector orientation (see discussion below). To further study this issue, detailed free energy calculations of the PS chains at interface are required, something which is beyond the scope of the present work. Furthermore, all model systems exhibit a very similar behavior; i.e., the increased polymer attraction which induced by the additional graphene layers does not seem to affect the orientation of the PS chains.

Data about the orientation of the end-to-end vector are shown in Figure 4b. It is also clear an almost parallel to the surface orientation for the $\mathbf{R}_{ee}$ vector for chains that are very close to graphene (i.e., for distances up to ∼5 Å) layers, whereas beyond this distance orientation of polymer chains is randomized abruptly. Chains appear to be slightly flattened also in the highly attenuated free surface region. Such a tendency of polymer chains to lie almost parallel to the free surface has been observed in the past in other polymer/vacuum interfaces and has been attributed to polymer cohesive forces.[38] Note, however, that for PS this tendency is clearly smaller than for a polymer with a simpler monomer structure, such as polyethylene or standard bead−spring polymer models.[17] This is directly related to the fact that, as discussed above, PS bulky side group adopt an almost perpendicular orientation in the PS/vacuum interface, and thus the chain's backbone (end-to-end vector) is not free enough to lie parallel to the free interface.

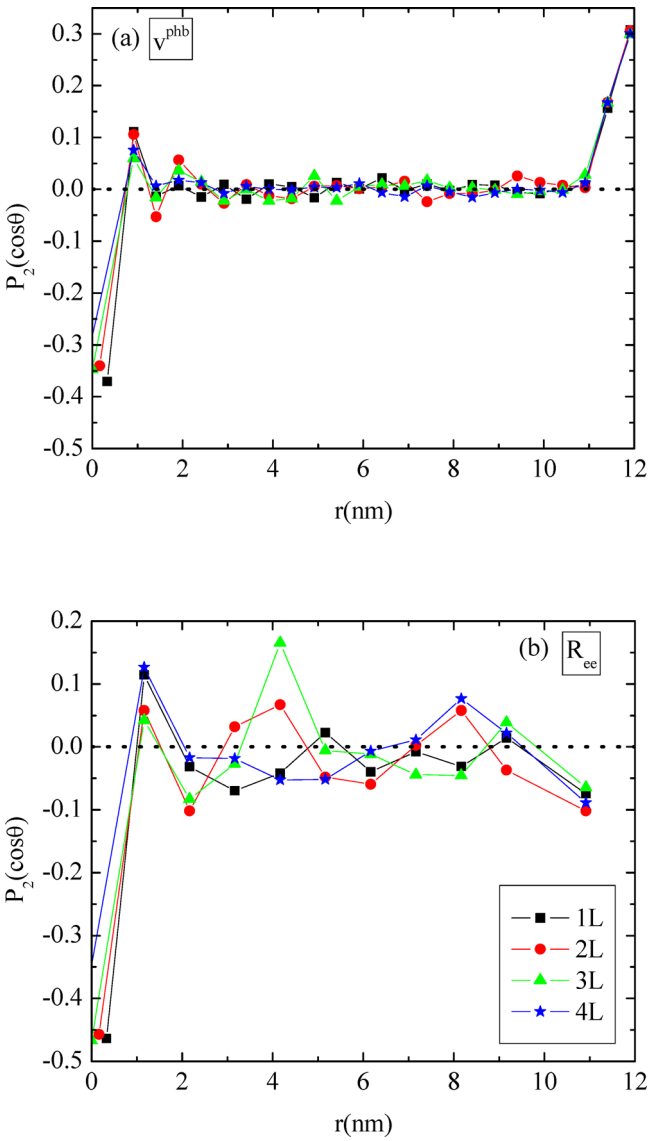


**Figure 4.** Second rank bond order parameter $P_2(\cos(\theta))$ of PS for all four systems as a function of the distance ($r$) from the closest to the polymer film graphene layer: (a) for the phelyl ring vector ($\mathbf{v}^{phb}$) and (b) for the end-to-end vector ($\mathbf{R}_{ee}$) of the polymer chain.

Our approach for the sorting of the various vectors (i.e., $\mathbf{v}_{bb}$ and $\mathbf{R}_{ee}$) in the different adsorption layers with respect to the surface is based on the center of mass of the corresponding vector. Note here that this approach for the case of the end-to-end vector might lead to selection bias, since only chains with a rather flat conformation will have their center of mass near the graphene sheet. An alternative approach would be to compute the mean end-to-end order parameter for each distance from the graphene by averaging over the order parameter for all chains, with a weighting assigned to each chain based on the fraction of monomers at a given distance from the graphene sheet that they belong to. Results for the two methods of analysis for the bond order parameter of the end-to-end vector of one model system (2L) are shown in Figure 6s of the Supporting Information. Only small differences are observed for the chains very close to the graphene sheet (first adsorption


DOI: 10.1021/ma502524e
Macromolecules XXXX, XXX, XXX−XXX

layer); i.e., $P_2$ is −0.45 from the first analysis and −0.3 from the second.

Additional information for the structure of PS chains close to the graphene surface is extracted from the calculation of the two-dimensional pair radial distribution function $g_{2D}(r)$ in the $xy$-plane (i.e., parallel to graphene) between monomers. Figure 7s in the Supporting Information presents the $g_{2D}(r)$ for all four systems together with the 4 times bigger system with one graphene layer. Although the statistics is rather poor, we can observe that no crystallization signs are present.

In order to better visualize the arrangement of polystyrene chains close to graphene layers, typical chain configurations of the model systems are presented in Figures 5b and 5c. First, in

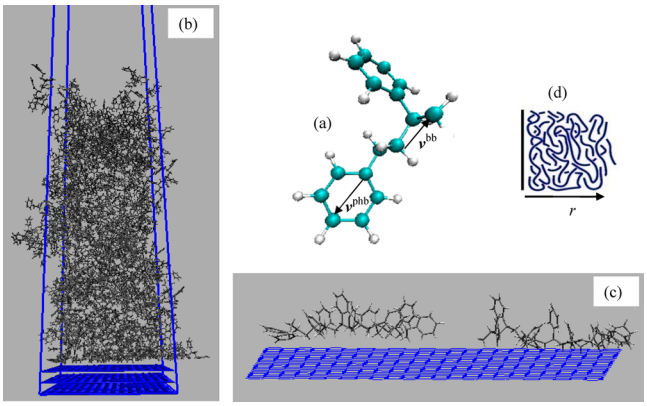


**Figure 5.** (a) Snapshot of an oligomer of PS where two characteristic vectors ($\mathbf{v}^{bb}$ and $\mathbf{v}^{phb}$) are drawn. (b) Snapshot of a model graphene/PS/vacuum system with three graphene layers. (c) Orientation of two representative PS chains close to the top graphene layer is shown. (d) Sketch of the model polymer film where the position of the graphene layer and the direction of the increasing distance from the substrate are shown.

Figure 5b a representative snapshot from one of the supported thin (graphene/PS/vacuum) films with three graphene layers is shown. We clearly observe the two interfaces: the PS/graphene high density region at the bottom and the PS/vacuum low density one at the top. Second, the orientation of two representative PS chains close to the top graphene layer is shown in Figure 5c. It is also clear the tendency of the chain's backbone to lie parallel on the surface, whereas also most of the phenyl rings exhibit a parallel to the surface orientation. Finally, in Figure 5d a representative sketch of the model polymer thin films is shown with the position of the substrate at the left side, indicating also the increasing distance ($r$) from the surface toward the vacuum interface. In the following sections, most properties are calculated as a function of the distance $r$.

**c. Segmental Dynamics of Polymer Chains.** Here we present results concerning the dynamical properties of the PS chains in the four free-standing PS/graphene thin films studied here. Moreover, we examine the way that segmental and terminal-chain dynamics is differentiated at both PS/graphene and PS/vacuum interfaces. Recently we have examined the dynamic (nonhomogeneous) behavior of polystyrene chains confined between graphene layers as a function of the distance from the graphene layers.[16] For such systems strong dependence of the PS chain relaxation times on the actual position of the chains has been found; i.e., both segmental and end-to-end vector (terminal) relaxation times are found to be much larger for adsorbed polymer chains than for chains in the bulk regime. For the latter chains both segmental and terminal relaxation times are equal to those of a bulk system. Here we explore how such a spatial distribution of relaxation times (dynamical heterogeneity) is affected, if so, first by the existence of additional graphene layers and second by the free-vacuum surface.

Orientational dynamics is described though the calculation of the second Legendre polynomial: $P_2(t) = (3/2)\langle\cos^2\theta(t)\rangle - 1/2$, where $\theta(t)$ is the angle of a vector under consideration at time $t$ relative to its position at $t = 0$. To study the orientational dynamics of the polymer chains at the segmental level a vector parallel to the backbone of the polymer chain, which connects two nonconsecutive carbon atoms separated by one carbon (1−3), has been chosen ($\mathbf{v}^{bb}$) (Figure 5a). Results for the autocorrelation function, $P_2(t)$, as a function of time for the system with four graphene layers are presented in Figure 6. As

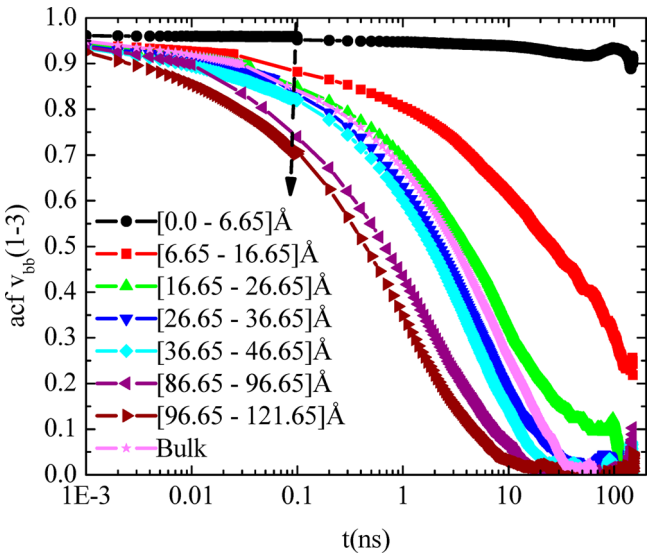


**Figure 6.** Time autocorrelation function of bond order parameter $P_2(t)$ as a function of time for the characteristic vector $\mathbf{v}^{bb}$ of PS for the system with four graphene layers. Arrows direction denotes the increasing distance from graphene layers. Widths of the various regimes are discussed in the text (see also legend of Figure 9b).

mentioned above, in this graph polymer chains were analyzed as a function of distance from the graphene layers by defining layers of 1 nm. Different curves correspond to different distances from the closest to the polymer graphene sheet and define a series of (adsorption) layers. The arrow's direction shows from the graphene toward the vacuum interface. As expected, a faster relaxation of the PS chains is observed with the increasing distance from graphene. In more detail, chains in the first, and less in the second, adsorption layer exhibit a much slower relaxation. Then, there is an intermediate region (∼4.0−9.5 nm) in which PS chains exhibit very similar dynamical behavior, which can be though as a "bulk-like regime", though it is not identical to the dynamics of the corresponding bulk system, as it will be discussed in more detail in the following. Finally, at the vacuum interface (∼9.5−13 nm) dynamics of PS chains becomes much faster than in the bulk. Qualitatively similar behavior has been observed also for the other systems studied here. Note that in the analysis performed here the relaxation of different vectors has been averaged over all of them within a specific adsorption layer. The further analysis of the dependence of the segmental $\alpha$-relaxation on the position


DOI: 10.1021/ma502524e
Macromolecules XXXX, XXX, XXX−XXX

of a vector along the chain's contour length is a very interesting issue. However, this requires the computation of the whole distribution of segmental relaxation times as well as extensive long time simulations of very large atomistic systems in order to get statistically accurate results, as shown in a recent study of the dynamics of PS−PI miscible polymer blends;[62] this will be part of a future work.

The mobility of the polymer chains can be further quantified by calculating the segmental relaxation time of the $\mathbf{v}^{bb}$ vector. We fit each curve with a Kohlrausch−Williams−Watts (KWW) stretch exponential function[63] of the form

$$P_2(t) = A \exp\left[-\left(\frac{t}{\tau_{KWW}}\right)^{\beta}\right]$$

where $A$ is a pre-exponential factor which takes into account relaxation processes at very short times (i.e., bond vibrations and angle librations), $\tau_{KWW}$ is the KWW relaxation time, and $\beta$ the stretch exponent, which describes the broadness of the distribution of the relaxation times (i.e., the deviation from the ideal Debye behavior: $\beta = 1$). The segmental relaxation time, $\tau_{seg}$, is calculated as the integral of the KWW curves through $\tau_{seg} = (\tau_{KWW}/\beta)\Gamma(1/\beta)$, where $\Gamma(\ )$ is the gamma function. Segmental relaxation times as a function of the distance ($r$) from the closest graphene sheet for all the systems are depicted in Figure 7a. Error bars of these calculations are of the order of 10−20% of the actual value being larger for the chains in distances closest to the graphene layers. Nevertheless, we have to note here that at the first adsorption layer the uncertainty in $\tau_{seg}$ values is even higher and can be about 100% of the actual values, which is not surprising if we consider that such time scales are out of the time window of the current MD simulations. For this reason the corresponding points for all four systems in Figure 6a are presented differently from the rest curves (open symbols) and are used only as indicators of the trend of each curve (i.e., very large relaxation times close to graphene layers which decrease systematically with the distance from the surface). An increase of relaxation times with the number of graphene sheets is observed at the first two or three adsorption layers, as expected; however, the differences in $\tau_{seg}$ values among the systems for the case of the first adsorption layer are rather crude estimations and not accurate values because of the very large error bars. At the second adsorption layer the system with one graphene sheet is found to be faster than the rest systems by almost a factor of 2, whereas the differences among the rest systems are within error bars. The corresponding values of $\beta$ exponents are presented in Figure 7b. Lower $\beta$ values close to graphene and close to the vacuum indicate a broader distribution of relaxation times at the interfaces compared to the intermediate "bulk-like" region. Error bars of these calculations are about ±0.05 for $\beta$.

We have to mention here that the error estimation for both $\tau_{seg}$ and $\beta$ values is not a trivial issue. Standard block averaging techniques cannot be used, especially in the first adsorption layer, where a small fraction (about 5−10%) of the $\alpha$-relaxation process has been realized. Thus, our estimation for the propagation of error due to fits uncertainties is based on an analysis of the fit of the curves with modified KWW functions using various combinations of the three fitting parameters. The ±0.05 value for $\beta$ corresponds to distances very close to the surface; therefore, it constitutes an upper limit (i.e., slightly overestimated for the rest of the film). $\beta$-values that correspond

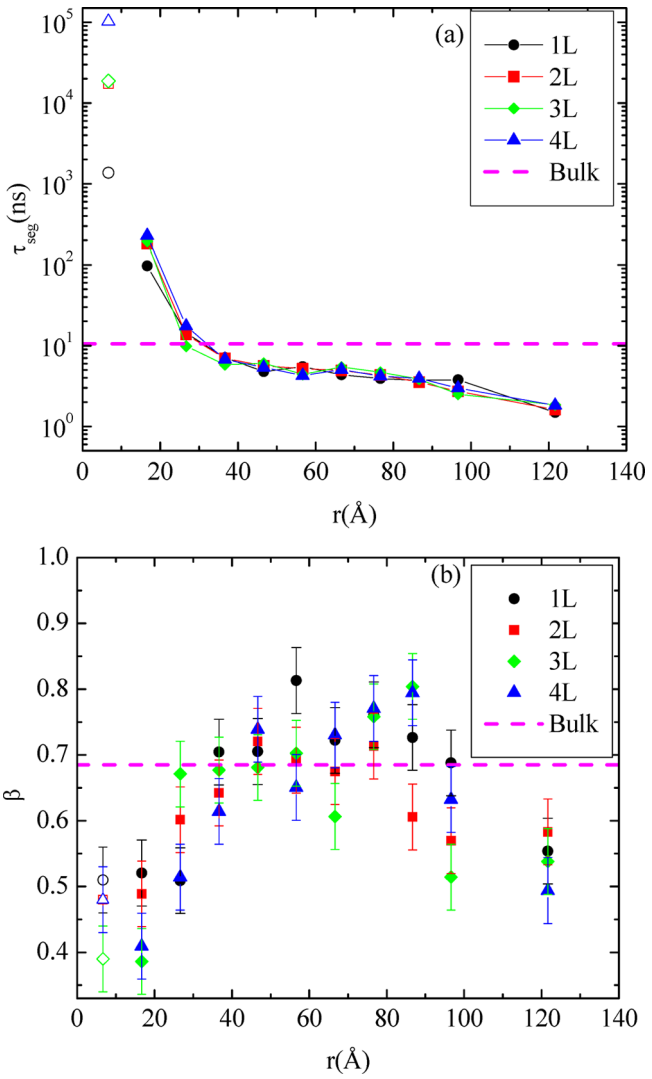


**Figure 7.** (a) Segmental relaxation time ($\tau_{seg}$) of $\mathbf{v}^{bb}$ vector of PS as a function of the distance ($r$) from the closest to the polymer film graphene layer for all four systems. (b) The corresponding stretch exponents, $\beta$, as a function of the distance ($r$) for all four systems, as extracted from the fit with KWW functions. Dashed lines represent $\tau_{seg}$ and $\beta$ of bulk PS at the same conditions.

to the first adsorption layer are presented with open symbols as well.

On top of that and in order to have an estimation of the effect of the number of graphene layers on the chain (segmental and end-to-end vector) relaxation at distances close to the interface, we compare the autocorrelation function of both $\mathbf{v}_{bb}$ and $\mathbf{R}_{ee}$ vectors at the first adsorption layer among the four systems. Data are presented in Figures 1sa and 1sb of the Supporting Information, respectively. Despite the fact that only a small fraction of the chain relaxation process has been realized, the curves show that orientational dynamics is faster in the one graphene layer system compared to the rest three systems in both segmental and entire chain level, whereas it is slower for the four graphene layer system.

Overall, it is clear that based on the data shown in Figure 7a one can roughly distinguish four regimes for the PS segmental dynamics, for all systems studied here, with respect to the distance from graphene: (a) First, polymer chains very close (up to ∼0.3−0.4 nm) to the graphene layers are practically


DOI: 10.1021/ma502524e
Macromolecules XXXX, XXX, XXX−XXX

immobile ("frozen") for the *time window* of the current MD simulations; their average segmental relaxation time is of the order of $10^5$ ns, about 4 orders of magnitude larger than of the bulk system. (b) Second, for longer distances from the surface (up to ∼3−4 nm) there is a considerable slowdown of chain dynamics with respect to the bulk PS systems. (c) Third, a "bulk-like" regime follows (distances ∼4.0− 9.5 nm) where the chain dynamics is almost independent of $r$. (d) Finally, a regime (∼9.5−13 nm) with much faster PS chain mobility at the PS/vacuum interface appears.

We should also note here that the increase of the relaxation time with the increase of the number of graphene layers in the first adsorption layer would lead to an increase in the average segmental relaxation time for the entire thin film. This would expect to lead to an increase in the average $T_g$ of the thin film as the number of graphene layers increases. This is in agreement with recent experimental[52] and simulation works using coarse-grained models[40,46,53] that predict an increase of the average $T_g$ of the thin film as the interfacial adhesive energy increases.

Furthermore, in order to directly compare the dynamics of the free-standing PS/graphene thin films with bulk PS systems, we also present in Figures 6, 7a, and 7b the corresponding data for a bulk polystyrene system with similar molecular length studied at the same temperature. From the data shown in Figures 6 and 7a we observe that the bulk curve/points do not coincide with the "bulk-like" region of the thin films; the latter is slightly more mobile (segmental relaxation time is smaller) than the corresponding bulk system. Moreover, throughout the "bulk-like" region there is also a weak dependence of the segmental relaxation times on the distance from the vacuum interface, such as the closer to the vacuum layers the faster their dynamics. Data concerning the stretch exponent $\beta$ are within the error bars.

The above dynamical behavior of the "bulk-like" regime of the PS thin films supported by graphene is clearly different than that of the "bulk-like" regime of the same PS system confined between graphene layers (with very similar width of the thin film); the latter one is very similar to the one of the bulk system.[16] The fact that the dynamics of the "bulk-like" regime of the free-standing films is slightly more mobile than the same regime of the confined system is a direct result of the PS/vacuum interface. This proves that the effect of the free surface on the polymer dynamics is not seen only in the region in which the density is considerable lower than in the bulk, but it is further extended in the thin film (although in a much weaker way), even in regions in which the polymer density is exactly the same as in the bulk. Note that according to our knowledge accelerated dynamics in the central film area of a supported film relative to bulk has not been observed before through detailed all-atom simulations. However, it has been recently founded by Hanakata et al.[26] using coarse-grained molecular dynamics simulations that relaxation time of the polymer chains on smooth surface decreases as the film thickness is decreased, relative to the corresponding bulk values, whereas an opposite behavior was found for rough surfaces. Moreover, we would naturally expect that for thicker films there will be less influence of the free surface on the central film area. Clearly more work is required to clarify the combined effects of smooth/rough surfaces, film dimensions, and specificity of polymer−solid interactions on the dynamics/friction at the atomistic level.

The above-discussed behavior is in qualitative agreement with recently proposed three-layer models that are introduced in order to describe the dynamics of free-standing polymer films as it is measured through analysis of the capillary waves.[21,24,31,34] According to this model, there is a strong adsorbed polymer layer that is almost frozen, a bulk regime, and a regime of high chain mobility at the free surface. A possible explanation of this effect could be the propagation of the high mobility of polymer chains at the free surface in the rest of the film through long-range hydrodynamic interactions. However, a detailed examination of this hypothesis requires a systematic study over various temperatures and molecular lengths. This will be the subject of a future work. Finally, we should state that this is in contrast to the structural aspects of thin films (e.g., density and chain conformations), for which there is a clear bulk region with properties identical to the bulk system corresponding ones.

**d. Terminal Dynamics of Polymer Chains.** Next, results concerning orientational as well as translational terminal-chain dynamics are presented. The molecular chain end-to-end vector relaxation time ($\tau_{mol}^{R_{ee}}$) is calculated for all four systems as a function of the distance from the interfaces. These calculations are based on the end-to-end vector autocorrelation function $u(t) = (\langle \mathbf{R}_{ee}(t)\cdot\mathbf{R}_{ee}(0)\rangle)/\langle \mathbf{R}_{ee}{}^2\rangle_0$ which provides information for the orientational dynamics in the entire chain level. $\mathbf{R}_{ee}(t)$ and $\mathbf{R}_{ee}(0)$ are the end-to-end distances at time $t$ and 0, respectively, and $\langle \mathbf{R}_{ee}^2\rangle_0$ is the mean-squared value of the equilibrium (unperturbed) end-to-end distance. As in the case of the segmental dynamics, a fit with KWW functions is performed on all the curves and the chain relaxation time, $\tau_{mol}^{R_{ee}}$, is calculated as $\tau_{mol}^{R_{ee}} = (\tau_{KWW}/\beta)\Gamma(1/\beta)$. Results for the molecular relaxation times and the corresponding $\beta$ exponents are depicted in Figures 8a and 8b, respectively. Error bars in these data are about $\pm$[0.05−0.1] for $\beta$ and of the order of 20−30% for $\tau_{mol}^{R_{ee}}$. Data for the dynamics of the bulk PS systems are also shown with dashed lines. Molecular relaxation times are as expected longer than the segmental ones, and they attain very large values close to the graphene surface which decrease gradually with the distance. Especially in the first adsorption layer (up to about 0.5 nm from the graphene layers) the calculated values for $\tau_{mol}^{R_{ee}}$ are extremely large, in practice beyond the time window of the simulation runs. The error bars for these values are also very large so we should discuss them more as a rough estimation of the slowdown of the chain dynamics close to the graphene layers rather than as accurate absolute numbers. The differences in $\tau_{mol}^{R_{ee}}$ values among the four systems, shown in Figure 8a, cannot be accurately quantified due to the very large uncertainties at distances close to the surface (i.e., here, the first and the second adsorption layer). For the rest of the film orientational terminal dynamics is qualitatively similar to the segmental one: The very large relaxation times are followed by a "bulk" region between 5 and 9 nm and a final acceleration beyond 9 nm, at the vacuum interface. On top of that, the value for the corresponding molecular relaxation time for a bulk system, included in Figure 8a (horizontal dashed line), is higher than the "bulk-like" value of the interfacial system (i.e., almost double). This is in agreement with the segmental relaxation time data discussed before (see Figure 7a), which indicates a shift of the "bulk-like" region toward smaller relaxation times. $\beta$ exponents attain higher values than the corresponding segmental curves and in the "bulk" region are ∼[0.8−0.9], similar to the value of the bulk system. However, values of the $\beta$ exponents close to the interfaces are much smaller (∼0.4−0.6), indicating a broader distribution of relaxation times at these distances.


DOI: 10.1021/ma502524e
Macromolecules XXXX, XXX, XXX−XXX

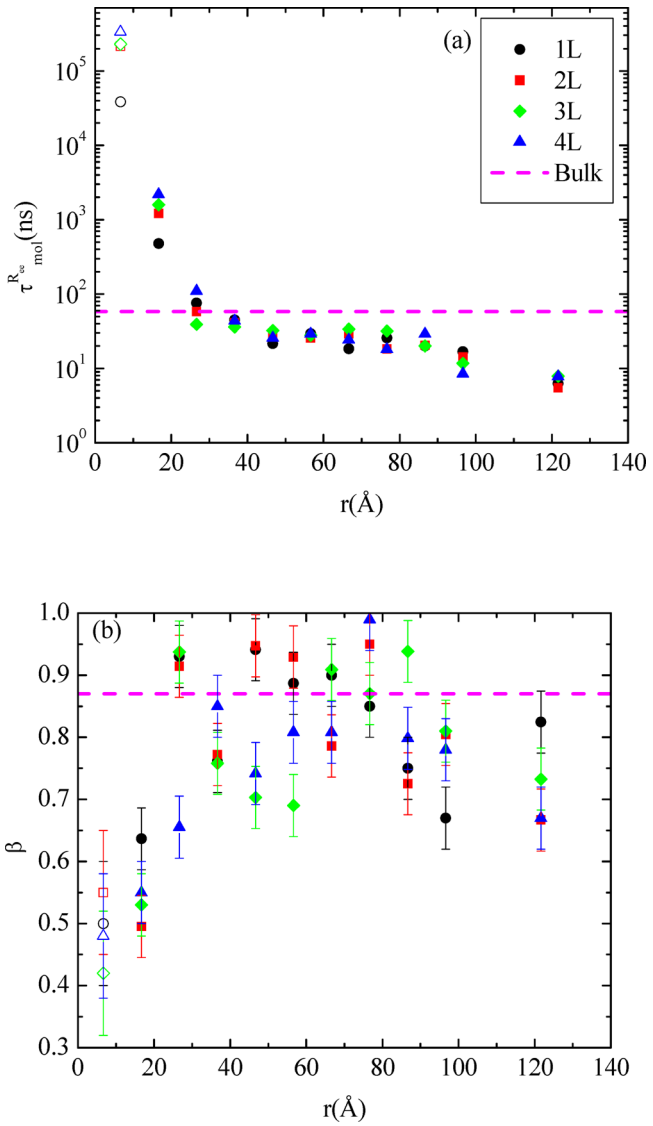


**Figure 8.** (a) Molecular relaxation time ($\tau^{R_{ee}}_{mol}$) of the end-to-end characteristic vector, $\mathbf{R}_{ee}$, of PS as a function of the distance ($r$) from the closest to the polymer film graphene layer for all four systems. (b) The corresponding stretch exponents, $\beta$, as a function of the distance ($r$) for all four systems, as extracted from the fit with KWW functions. Dashed lines represent $\tau^{R_{ee}}_{mol}$ and $\beta$ of bulk PS at the same conditions.

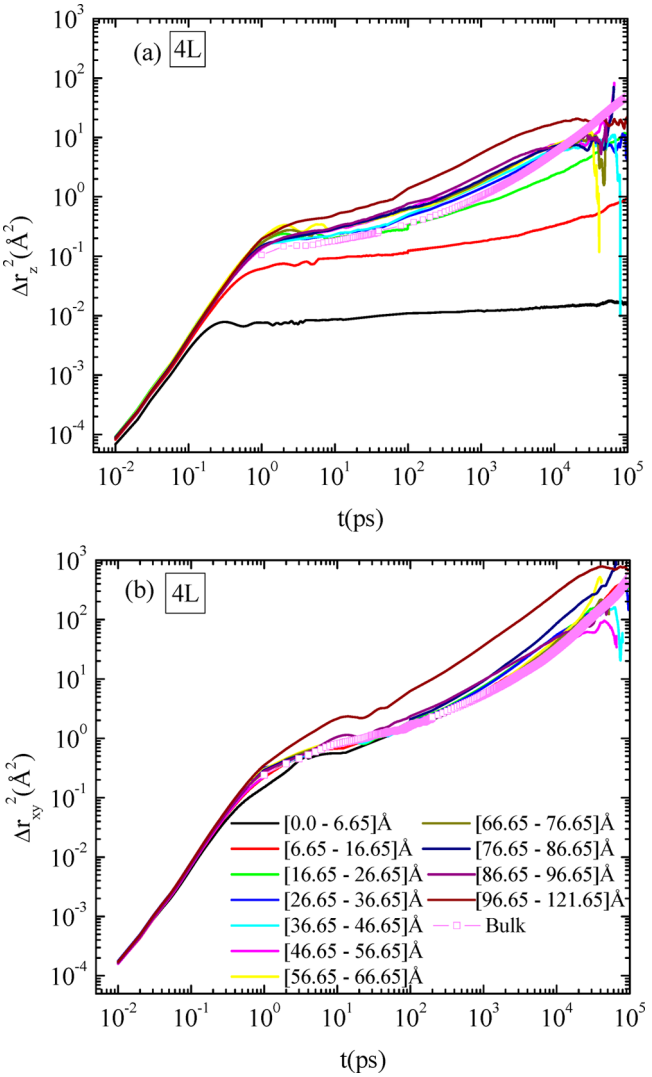


**Figure 9.** Mean-squared displacement of the chain's center of mass as a function of time at different distances from the closest to the polymer film graphene layer for the system with four graphene layers: (a) the $z$-component (perpendicular to the surface) and (b) the $xy$-component (in-plane motion).

Finally, translational dynamics in the entire chain level is studied through the calculation of the mean-squared displacement (msd) of the center of mass of the polymer chain, $\Delta\mathbf{R}_{CM}^2 = \langle(\mathbf{R}_{CM}(t) - \mathbf{R}_{CM}(0))^2\rangle$, where $\mathbf{R}_{CM}$ is the position of the chain's center of mass. In a recent MD simulation study[16] on a polystyrene film confined between two graphene layers, we have observed homogeneous dynamics for the in plane motion ($xy$-direction) at any distance from the surface. Differentiations as a function of the distance from graphene were presented in the perpendicular to the surface motion ($z$-direction). The mean-squared displacement of the chain's center of mass is depicted in Figures 9a and 9b for the $z$- and the $xy$-component, respectively. Data shown in these figures are obtained from the analysis of the thin film with four graphene layers; however, the behavior is similar for the other systems. We observe that normal to the interfaces the effect is qualitatively the same as in the orientational dynamics (i.e., both segmental and terminal autocorrelation functions). For the very short times the dynamics for all segments is as expected similar (ballistic motion), and the differences appear for longer times. Graphene layer affects strongly the dynamics, hindering the motion up to ~2 nm, then an almost bulk region is observed which is again moved to larger values compared to the corresponding bulk curve (i.e., faster dynamics), and a final speed-up at the vacuum interface appears. For the in plane motion dynamics is homogeneous throughout the film and identical to the one of the corresponding bulk system, except for the free surface where dynamics is again faster. It is interesting to observe that the $z$-component of $\Delta\mathbf{R}_{CM}^2$ (Figures 9a) attains a plateau, more pronounced in the first two adsorption layers, which predisposes for a glassy-like regime for the chains very close to the graphene layers. However, a considerable in plane diffusion (Figures 9b) of polymer chains is observed ($xy$-direction) which proves that the total behavior of polymer is not that of glass even at distances very close to the substrate. This shows that the polymer−graphene interaction affects


DOI: 10.1021/ma502524e
Macromolecules XXXX, XXX, XXX−XXX

strongly *only* the motion vertical to the graphene interface, but it does not induce typical glass dynamics.

We have seen that the vacuum affects strongly the dynamic properties of the polymer chains, for the thin films considered here, increasing their mobility—an effect that propagates from the vacuum to the film resulting in a modified "bulk-like" region. Concerning the differences among the systems with a different number of graphene sheets, we focus on the two interfaces. In Figures 10a and 10b the *z*-component of the

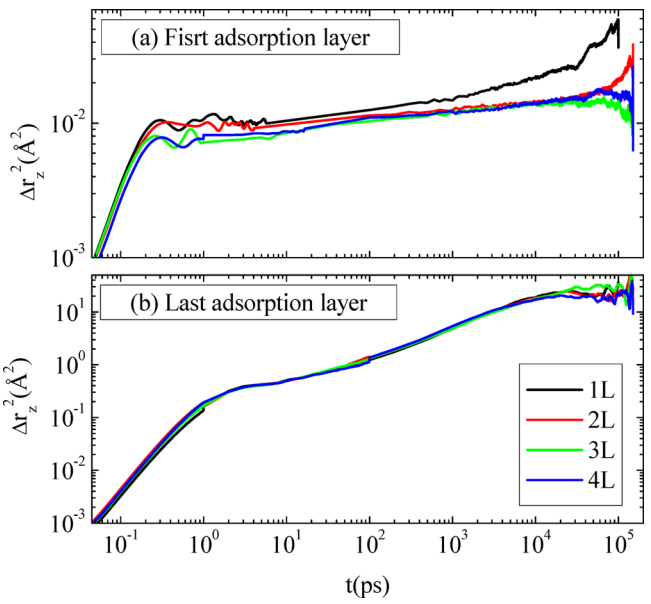


**Figure 10.** Mean-squared displacement of the chain's center of mass as a function of time at different distances from the closest to the polymer film graphene layer for all four systems: (a) at the first adsorption layer (closest to the graphene layers) and (b) at the last adsorption layer (PS/vacuum interface).

mean-squared displacement of the center of mass of the polymer chain is presented for the four systems at the first adsorption layer (i.e., graphene interface) and at the last adsoprion layer (i.e., vacuum interface). Differences are mainly identified between the system with the one graphene sheet and the rest of the systems. In the first adsorption layer (Figure 10a) systems with two, three, and four graphene sheets are equally slower than the system with the one graphene sheet. This observation is consistent with the increase in the PS/graphene (attractive) interaction energy (Figure 1) as the number of the graphene layers increases. In addition, the divergence in msd curves becomes larger with time, and only for very short times (ballistic regime) they are on top of each other since they do not "feel" the effect of the graphene layers. On the other hand, at the vacuum interface (Figure 10b) no differentiation in the diffusion exists among the four systems.

Note here that a similar qualitative behavior is observed in the segmental level as well. Both the *z*- and *xy*-components of the segmental mean-squared displacement are depicted in Figures 8sa and 8sb of the Supporting Information, respectively, for the system with four graphene layers. Four representative curves throughout the film are presented, where again a plateau is observed at distances close to the interface (i.e., the first two adsorption layers) for the vertical to the surface diffusion. However, the in-plane diffusion is significant as in the case of the terminal dynamics.

## 4. CONCLUSIONS

The present work focuses on the way that two different interfaces (PS/graphene and PS/vacuum) affect the various properties of thin polystyrene films. The systems have been studied are thin PS films (i.e., ∼12 nm, that is about $17R_g$) supported by multiple (one to four) graphene layers. The properties of the systems are examined as a function of the adhesive PS/graphene interaction energy (i.e., attraction), which increases (in absolute values) with the number of the layers. On top of that, properties of polymer chains are presented as a function of the distance from the interfaces. In the current study the range of the effect of each of the interfaces on the density, the structural and the dynamical properties of PS has been examined.

Both PS/graphene and PS/vacuum interfaces affect the polymer's behavior, though in a different way. In more detail, concerning (monomer) mass density profiles a maximum density peak is observed, which increases as the number of the graphene layers increases from one to four, as a result of the increasing interaction strength between the polymer and the graphene surface at very close distances (i.e., ∼0.3−0.4 nm from the closest graphene layer). At longer distances (i.e., ∼2−10 nm) the bulk density value is attained from all four systems, whereas a final decrease following a typical sigmoidal shape is observed at the vacuum interface (i.e., ∼10−12 nm). An obvious preference of the end monomers for both interfaces is also detected in all cases.

Structural and *conformational heterogeneities* of polymer chains were further analyzed both in segmental and entire chain level, through the calculation of the second Legendre polynomial, $P_2(\cos(\theta))$, for a vector from the backbone to the phenyl ring ($\mathbf{v}^{phb}$) and for the end-to-end vector ($\mathbf{R}_{ee}$) of the PS chain. Similar behavior for all systems was observed: A tendency for an almost parallel to the graphene surface orientation of the rings at very close distances (∼0.5 nm) was shown, whereas at longer distances their orientation is randomized. At the vacuum interface (i.e., ∼11−12 nm) a completely opposite behavior is observed; i.e., phenyl rings stick out into the vacuum phase in an almost perpendicular orientation. The orientation of the backbone of the polymer chain is examined through the characteristic end-to-end vector ($\mathbf{R}_{ee}$). At the graphene interface the parallel to the surface chain orientation is very pronounced for all the systems. The chain's backbone orientation is randomized as the distance from the substrate increases, whereas a small tendency for a flattened orientation is also appeared at the vacuum interface.

The effect of the polymer/graphene interfaces is of great importance on the dynamical properties of the polymer. *Dynamical heterogeneities* due to polymer/graphene and polymer/vacuum interfaces have been examined in detail in the level of both segmental and terminal dynamics. The segmental relaxation time ($\tau_{seg}$) calculated for a vector defined along the backbone of the chain ($\mathbf{v}^{bb}$) presents a four-regime behavior. Very close to the graphene layer (∼0.3−0.4 nm) the PS/graphene adhesive interaction results in very large $\tau_{seg}$ values of about 4 orders of magnitude larger than the bulk ones (practically out of the time window of the current simulations). In the range of ∼3−4 nm a gradual slowdown of chain dynamics, compared to the bulk values, is shown, whereas a plateau ("bulk-like" regime ∼4.0−9.5 nm) follows in which $\tau_{seg}$ is almost constant. Finally, a speed-up of chain dynamics is observed in the regime of ∼9.5−13 nm, very close to the free


DOI: 10.1021/ma502524e
Macromolecules XXXX, XXX, XXX−XXX

surface. On top of that a differentiation among the four systems is observed up to the third adsorption layer (~3 nm), where the more the graphene layers, the slower the dynamics. This is attributed to the stronger interactions between the polymer and the substrate. For the rest of the film dynamics are identical for the four systems.

A particular important observation concerns the "bulk-like" regime of PS segmental dynamics. In this regime $\tau_{seg}$ values do not coincide with the $\tau_{seg}$ value of a corresponding bulk system, which is the case for the bulk-like regime of a confined polymer film between graphene layers as well, but it is smaller, indicating a slightly higher mobility of the PS chains in the "bulk-like" regime for the free-standing films. This is a consequence of the PS/vacuum interface and is in qualitative agreement with three layers models that recently have been proposed. Nevertheless, this result nominates further investigation as a function of temperature, molecular weight, and width of the thin film, and it will be the subject of a future work. The values for $\beta$ exponents also indicate a broader distribution of relaxation times at both interfaces, whereas in the intermediate region they are close to the corresponding bulk value within error bars.

Qualitatively similar to the above-discussed behavior has been observed for the terminal orientational dynamics, which is studied through the characteristic end-to-end vector, $\mathbf{R}_{ee}$. The four regimes with respect to the distance between the two interfaces for the chain relaxation time, $\tau_{mol}^{\mathbf{R}_{ee}}$, are observed at the same intervals as the ones of $\tau_{seg}$, though their values are about 1 order of magnitude higher. Moreover, a bulk regime of slightly higher mobility compared to the bulk system is present here as well. Finally, the corresponding $\beta$ exponents attain higher values compared to the segmental ones in the range of 0.8−0.9 in the "bulk region", very similar to that of the bulk system.

Translational terminal dynamics was studied both for the in-plane motion (*xy*-direction) and perpendicular to the surface (*z*-direction). Normal to the interfaces a behavior qualitatively similar to the orientational one is observed; i.e., a clear slowdown of chain dynamics for chains up almost ~2 nm from the graphene layers, then a "bulk regime" follows, and finally at the PS/vacuum interface the terminal dynamics of the PS chains is much faster compared to the bulk one. A comparison among the thin PS films supported by multiple graphene layers indicates a difference in the PS chain mobility mainly for the system with one graphene layer and only at the PS/graphene interface: The one layer system is faster (for the motion normal to the surface, *z*-direction) compared to the rest three systems for which the diffusion is almost identical. The in-plane (*xy*-) mobility of the PS chains is the same for all PS chains independent of their spatial position, but the PS/vacuum (free) interface where, due to more available free volume, faster chain dynamics is observed.

One of the main results of the present work is the qualitative differences among the (in plane) translational and orientational dynamical behavior of the PS chains at the PS/graphene interface, discussed above. Note also that similar behavior has been seen for other polymer/graphene[16] and polymer/metal systems.[64] Such observations arise even more (open) questions related to the whether polymer chains physically adsorbed (due to attractive dispersion interactions) at a solid substrate exhibit "glassy-like" dynamics. Undoubtedly, more data from detailed atomistic simulations, as well as experimental approaches, for the dynamics of polymer thin films, over various polymer/solid systems, molecular weights and temperatures are required to clarify these issues.

Overall, PS chains exhibit strong dynamical heterogeneities with respect their translational and orientational motion along the entire polymer thin film. Future plans concern a detailed analysis of the dynamics as a function of the thickness of the thin films, the molecular weight of the polymer chains, and the temperature. On top of that study of different polymer thin films supported by graphene, or functionalized graphene, will be performed in order to further examine the role of specific interactions on the dynamical behavior of the polymer chains.

## ■ ASSOCIATED CONTENT

### Ⓢ Supporting Information

Figures 1s−8s. This material is available free of charge via the Internet at http://pubs.acs.org.

## ■ AUTHOR INFORMATION


### Corresponding Authors

*E-mail: rissanou@tem.uoc.gr; Ph +30 2810393746; Fax +30 2810393701 (A.N.R.).

*E-mail: vagelis@tem.uoc.gr; Ph +30 2810393735; Fax +30 2810393701 (V.H.).


### Notes

The authors declare no competing financial interest.

## ■ ACKNOWLEDGMENTS

This research has been cofinanced by the European Union (European Social Fund − ESF) and Greek national funds through the Operational Program "Education and Lifelong Learning" of the National Strategic Reference Framework (NSRF) − Research Funding Programs: KRHPIS and ARISTEIA II. We also thank manuscript referees for their constructive comments.

## ■ REFERENCES


(1) Catro-Neto, A. H.; Guinea, F.; Peres, N. M. R.; Novoselov, K. S.; Geim, A. K. *Rev. Mod. Phys.* **2009**, *81* (1), 109.

(2) Tsoukleri, G.; Parthenios, J.; Papagelis, K.; Jalil, R.; Ferrari, A. C.; Geim, A. K.; Novoselov, K. S.; Galiotis, C. *Small* **2009**, *5*, 2397.

(3) Novoselov, K. S.; Geim, A. K.; Morozov, S. V.; Jing, D.; Zhang, Y.; Dubonos, S. V.; Grigorieva, I. V.; Firsov, A. A. *Science* **2004**, *306* (5696), 666.

(4) Kim, H.; Abdala, A. A.; Macosko, C. W. *Macromolecules* **2010**, *43*, 6515.

(5) Wang, G. X.; Shen, X. P.; Yao, J.; Park, J. *Carbon* **2009**, *47*, 2049.

(6) Butt, H. J.; Duran, H.; Egger, W.; Faupel, F.; Harmandaris, V.; Harms, S.; Johnston, K.; Kremer, K.; Lin, F. Y.; Lue, L.; Ohrt, C.; Raetzke, K.; Ravelli, L.; Steffen, W.; Vianna, S. D. B. *Macromolecules* **2014**, *47*, 8459.

(7) Fleer, G. J.; Cohen Stuart, M. A.; Scheutjens, J. M. H. M.; Cosgrove, T.; Vincent, B. *Polymers at Interfaces*; Chapman & Hall: London, 1993.

(8) Jones, R. A. L.; Richards, R. W. *Polymers at Surfaces and Interface*; Cambridge University Press: Cambridge, 1999.

(9) Zheng, X.; Rafailovich, M. H.; Sokolov, J.; Strzhemechny, Y.; Schwarz, S. A.; Sauer, B. B.; Rubinstein, M. *Phys. Rev. Lett.* **1997**, *79*, 241.

(10) Frank, B.; Cast, A. P.; Russel, T. P.; Brown, H. R.; Hawker, C. *Macromolecules* **1996**, *29*, 6531.

(11) Lin, E.; Wu, W.; Satija, S. *Macromolecules* **1997**, *30*, 7224.

(12) Anastasiadis, S. H.; Karatasos, K.; Vlachos, G.; Manias, E.; Giannelis, E. P. *Phys. Rev. Lett.* **2000**, *84*, 915.

(13) Fotiadou, S.; Chrissopoulou, K.; Frick, B.; Anastasiadis, S. H. *J. Polym. Sci., Part B: Polym. Phys.* **2010**, *48*, 1658.




DOI: 10.1021/ma502524e
*Macromolecules* XXXX, XXX, XXX−XXX

(14) Rissanou, A. N.; Harmandaris, V. *J. Nanopart. Res.* **2013**, *15*, 1589:1.
(15) Rissanou, A. N.; Harmandaris, V. *J. Macromol. Symp.* **2013**, *331*−*332*, 43.
(16) Rissanou, A. N.; Harmandaris, V. *Soft Matter* **2014**, *10*, 2876.
(17) Harmandaris, V. A.; Daoulas, K. C.; Mavrantzas, V. G. *Macromolecules* **2005**, *38*, 5780; *Macromolecules* **2005**, *38*, 5796.
(18) Harmandaris, V.; Kremer, K. *Macromolecules* **2009**, *42*, 791; *Soft Matter* **2009**, *5*, 3920.
(19) Mansfield, K. F.; Theodorou, D. N. *Macromolecules* **1989**, *22*, 3143; *Macromolecules* **1991**, *24*, 4295.
(20) Bitsanis, I. A.; Hatziioannou, G. *J. Chem. Phys.* **1990**, *92*, 3827.
(21) Yang, Z.; Fujii, Y.; Lee, F. K.; Lam, C.-H.; Tsui, O. K. C. *Science* **2010**, *328*, 1676.
(22) Baljon, A. R. C.; Williams, S.; Balabaev, N. K.; Paans, F.; Hudzinskyy, D.; Lyulin, A. V. *J. Polym. Sci., Part B* **2010**, *48*, 1160.
(23) Priestley, R. D.; Ellison, C. J.; Broadbelt, L. J.; Torkelson, J. M. *Science* **2005**, *309*, 456.
(24) Chai, Y.; Salez, T.; McGraw, J. D.; Benzaquen, M.; Dalnoki-Veress, K.; Raphaël, E.; Forrest, J. A. *Science* **2014**, *343*, 994.
(25) Tress, M.; Erber, M.; Mapesa, E. U.; Huth, H.; Müller, J.; Serghei, A.; Schick, C.; Eichhorn, K. J.; Voit, B.; Kremer, F. *Macromolecules* **2010**, *43* (23), 9937.
(26) Hanakata, P. Z.; Douglas, J. F.; Starr, F. W. *Nat. Commun.* **2014**, *5*, 4163.
(27) Madden, W. J. *J. Chem. Phys.* **1987**, *87*, 1405.
(28) Xia, W.; Mishra, S.; Keten, S. *Polymer* **2013**, *54*, 5942.
(29) Eslami, H.; Müller-Plathe, F. *J. Phys. Chem. C* **2013**, *117*, 5249.
(30) Tito, N. B.; Lipson, J. E. G.; Milner, S. T. *Soft Matter* **2013**, *9*, 9403.
(31) Yang, Z.; Clough, A.; Lam, C. H.; Tsui, O. K. C. *Macromolecules* **2011**, *44*, 8294.
(32) Koga, T.; Jiang, N.; Gin, P.; Endoh, M. K.; Narayanan, S.; Lurio, L. B.; Sinha, S. K. *Phys. Rev. Lett.* **2011**, *107*, 225901.
(33) Paeng, K.; Ediger, M. D. *Macromolecules* **2011**, *44*, 7034.
(34) Peng, D-d.; Li, R-x. N.; Lam, C-h.; Tsui, O. K. C. *Chin. J. Polym. Sci.* **2013**, *31*, 12.
(35) Mansfield, K. F.; Theodorou, D. N. *Macromolecules* **1991**, *24*, 6283.
(36) Yelash, L.; Virnau, P.; Binder, K.; Paul, W. *Europhys. Lett.* **2012**, *98*, 28006.
(37) Falkovich, S. G.; Larin, S. V.; Lyulin, A. V.; Yudin, V. E.; Kenny, J. M.; Lyulin, S. V. *RSC Adv.* **2014**, *4*, 48606.
(38) Tatek, Y. B.; Tsige, M. *J. Chem. Phys.* **2011**, *135*, 174708.
(39) Karatasos, K. *Macromolecules* **2014**, *47*, 8833.
(40) Lang, R. J.; Merling, W. L.; Simmons, D. S. *ACS Macro Lett.* **2014**, *3*, 758.
(41) Young, R. J.; Gong, L.; Kinloch, I. A.; Riaz, I.; Jalil, R.; Novoselov, K. S. *ACS Nano* **2011**, *5*, 3079.
(42) Hess, B.; Kutzner, C.; van der Spoel, D.; Lindahl, E. *J. Chem. Theory Comput.* **2008**, *4*, 435.
(43) Bussi, G.; Donadio, D.; Parinello, M. *J. Chem. Phys.* **2007**, *126*, 014101.
(44) Müller-Plathe, F. *Macromolecules* **1996**, *29*, 4782.
(45) Steele, W. A. *Surf. Sci.* **1973**, *36*, 317.
(46) Amit, S.; Riggleman, R. A. *J. Phys. Chem. B* **2014**, *118*, 9096.
(47) Lang, R. J.; Simmons, D. S. *Macromolecules* **2013**, *46*, 9818.
(48) Long, D.; Lequeux, F. *Eur. Phys. J. E: Soft Matter Biol. Phys.* **2001**, *4*, 371.
(49) Lipson, J. E. G.; Milner, S. T. *Eur. Phys. J. B* **2009**, *72*, 133.
(50) Rissanou, A. N.; Power, A. J.; Harmandaris, V. *Polymers* **2015**, *7*, 390.
(51) Harmandaris, V.; Foudas, G.; Kremer, K. *Macromolecules* **2011**, *44*, 393; *Phys. Rev. Lett.* **2013**, *110*, 165701.
(52) Fryer, D. S.; Peters, R. D.; Kim, E. J.; Tomaszewski, J. E.; Nealey, P. F. *Macromolecules* **2001**, *34*, 5627.
(53) Torres, J. A.; Nealey, P. F.; de Pablo, J. J. *Phys. Rev. Lett.* **2000**, *85*, 3221.
(54) Alexiadis, O.; Mavrantzas, V. G.; Khare, R.; Beckers, J.; Baljon, A. R. C. *Macromolecules* **2008**, *41*, 987.
(55) Hudzinskyy, D.; Lyulin, A. V. *Modelling Simul. Mater. Sci. Eng.* **2011**, *19*, 074007.
(56) Hudzinskyy, D.; Lyulin, A. V.; Baljon, A. R. C.; Balabaev, N. K.; Michels, M. A. J. *Macromolecules* **2011**, *44*, 2299.
(57) Kotelyanskii, M.; Theodorou, D. N. *Simulation Methods for Polymers*; Marcel Dekker Inc.: New York, 2004.
(58) Turzi, S. S. *J. Math. Phys.* **2011**, *52*, 053517−1.
(59) Clancy, T. C.; Dhinojwala, A.; Mattice, W. L. *J. Phys. Chem. B* **2001**, *105*, 11493.
(60) Gautam, K. S.; Schwab, A. D.; Dinojwala, A.; Zang, D.; Dougal, S. M.; Yeganeh, M. S. *Phys. Rev. Lett.* **2000**, *85*, 3854.
(61) Briggman, K. A.; Stephenson, J. C.; Wallace, W. E.; Richter, L. J. *J. Phys. Chem. B* **2001**, *105*, 2785.
(62) Harmandaris, V.; Doxastakis, M. *J. Chem. Phys.* **2013**, *139*, 034904.
(63) Williams, G.; Watts, D. C. *Trans. Faraday Soc.* **1970**, *66*, 80.
(64) Johnston, K.; Harmandaris, V. *Soft Matter* **2012**, *8*, 6320; *Macromolecules* **2013**, *46*, 5741.


DOI: 10.1021/ma502524e
*Macromolecules* XXXX, XXX, XXX−XXX